

Current effects and topology of current paths in single crystalline $\text{Pr}_{0.7}\text{Pb}_{0.3}\text{MnO}_3$

Run-Wei Li^{a)}*International Center for Young Scientists (ICYS), National Institute for Materials Science (NIMS), 1-1 Namiki, Tsukuba, Ibaraki 305-0044, Japan*Xin Zhou^{b)}*Max Planck Institute for Polymer Research, Ackermannweg 10, 55128 Mainz, Germany*Alexei A. Belik and Jun-ichi Inoue^{c)}*International Center for Young Scientists (ICYS), National Institute for Materials Science (NIMS), 1-1 Namiki, Tsukuba, Ibaraki 305-0044, Japan*

Kazushi Miki

Nanomaterials Laboratory (NML), National Institute for Materials Science (NIMS), 1-1 Namiki, Tsukuba, Ibaraki 305-0044, Japan

Bao-Gen Shen

State Key Laboratory of Magnetism, Institute of Physics, Chinese Academy of Sciences, P.O. Box 603, Beijing 100080, China and Center for Condensed Matter Physics, Chinese Academy of Sciences, P.O. Box 603, Beijing 100080, China

(Received 14 February 2006; accepted 31 August 2006; published online 6 December 2006)

In electron-phase-separated $\text{Pr}_{0.7}\text{Pb}_{0.3}\text{MnO}_3$ single crystals, nonlinear current effects have been observed above a critical current (I_c), beyond which a metal-insulator transition could be induced by the applied electrical current. We found that the square of I_c was linearly related to the external temperature, which can be well understood based on a local heating-cooling model. Furthermore, the surface area and mass of the current paths in the phase-separated systems were obtained by fitting our experimental data to the model, and a temperature-dependent topology of the current paths was found. In addition, interesting oscillatory behaviors in differential resistance (dV/dI) were observed at temperatures slightly above the metal-insulator transition temperature, which can be attributed to electron tunneling between isolated ferromagnetic clusters embedded in the insulating paramagnetic matrix. © 2006 American Institute of Physics. [DOI: 10.1063/1.2372762]

I. INTRODUCTION

Since the discovery of colossal magnetoresistive effects,^{1,2} perovskite manganites $\text{Ln}_{1-x}\text{A}_x\text{MnO}_3$ ($\text{Ln}=\text{La}, \text{Pr}, \text{Nd}, \text{etc.}$, $\text{A}=\text{Ca}, \text{Sr}, \text{Ba}, \text{Pb}, \text{etc.}$) have been studied extensively due to not only their rich physical properties but also their potential applications in magnetic memory and sensors. Usually, large magnetoresistance appears near a ferromagnetic-paramagnetic phase transition accompanied by a metal-insulator (MI) transition, as has been explained based on the double exchange model.³ In the double exchange model, the hopping of itinerant e_g electrons from trivalent Mn^{3+} to tetravalent Mn^{4+} sites facilitates both the ferromagnetism and metallic conductivity. Experimentally, some external factors such as magnetic field, electric field, and even hydrostatic pressure can affect the phase transition and transport properties.⁴ Recently, the effects of electrical current on both the phase transition and transport properties have attracted a large amount of interests^{5–21} particularly in charge-ordered systems.

In our previous studies,^{22,23} it was found that single

crystalline $\text{Pr}_{0.7}\text{Pb}_{0.3}\text{MnO}_3$ displays an electronic phase separation near the MI transition temperature (T_{MI}). With increasing temperature, this system experiences an unconventional sequence of phase transitions, ferromagnetic phase \rightarrow ferromagnetic + paramagnetic phase \rightarrow superparamagnetic + paramagnetic phase \rightarrow paramagnetic phase. The ferromagnetic phase \rightarrow ferromagnetic + paramagnetic phase transition takes place at the Curie temperature ($T_C \sim 205$ K), and the ferromagnetic + paramagnetic phase \rightarrow superparamagnetic + paramagnetic phase transition takes place at T_{MI} (~ 235 K). In the temperature region slightly above T_{MI} , a large low-field magnetoresistance due to spin-dependent electron tunneling between isolated ferromagnetic clusters was observed. Moreover, by combining voltage-current (V - I) and specific heat measurements, nonlinear current effects were observed, which indicates that a solely Joule heating process cannot be completely responsible for the nonlinear current effects.²⁴ V - I curves measured from 5 to 235 K are shown in Fig. 1 [and also Fig. 1(a) in Ref. 24]. When the temperature is below 150 K, V - I curves are linear up to 0.3 A. When the temperature is higher than 150 K, a nonlinear V - I behavior is observed. For example, at 170 K, the resistance (V/I) remains relatively constant below 0.15 A, then increases sharply up to $\sim 0.9 \Omega$, after that it decreases

^{a)}Electronic mail: runwei.li@nims.go.jp

^{b)}Electronic mail: xzhou@lanl.gov

^{c)}Present address: Quantum Dot Research Center, National Institute for Materials Science (NIMS), 1-1 Namiki, Tsukuba, Ibaraki 305-0044, Japan.

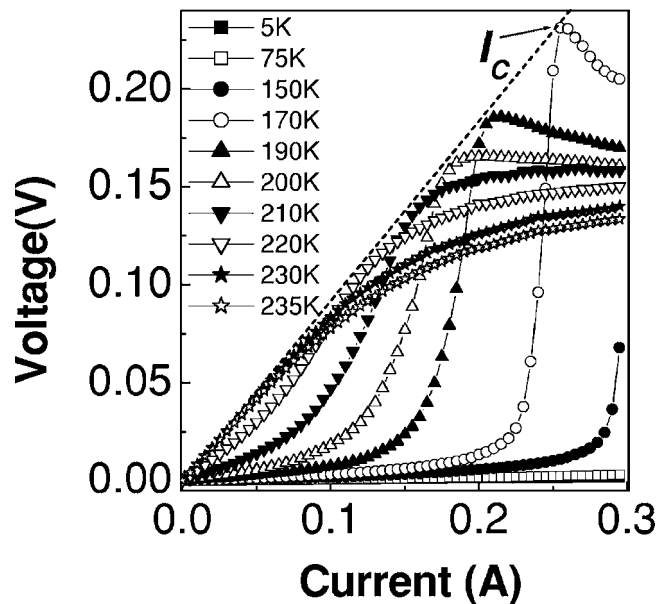


FIG. 1. V - I curves measured from 5 to 235 K. The dashed line, which indicates a resistance of 0.9Ω , is used as a guide to the eyes.

again upon increasing current. We define the current at which the resistance begins to decrease as the threshold current (as shown in Fig. 1).

In this article, based on a heat transport equation taking into account Joule heating and Newtonian cooling processes, we have derived the linear relationship between the square of the threshold current and the external temperature, which agrees well with the experimental results. Some information about the surface area and mass (volume) of current paths in the phase-separated systems has been obtained. Furthermore, oscillating behaviors in the differential resistance (dV/dI) were observed at temperatures slightly above T_{MI} .

II. EXPERIMENTAL DETAILS

The $\text{Pr}_{0.7}\text{Pb}_{0.3}\text{MnO}_3$ single crystals grown by the flux method have been used in our previous studies (Refs. 22–24). The size of the sample for V - I measurements was approximately $6 \times 2 \times 1.5 \text{ mm}^3$. dc V - I curves were measured using a standard four-probe method. Four Cu electrodes with a width of $\sim 0.4 \text{ mm}$ were prepared by thermal evaporation. For each V - I data point, two current pulses with duration of 1 s were used in opposite directions to obtain an average.

III. RESULTS AND DISCUSSIONS

As discussed in Ref. 24, the V - I and specific heat data indicated that the heating/conductance in the phase-separated sample was not uniform and that Joule heating only warmed part of the sample to T_{MI} . The nonuniformity of the heating/conductance might have come from two sources. One was the coexistence of two phases with different conductances. The other was nonuniform temperature distribution from the center to the boundary of the sample due to the cooling by the external environment. For the latter, if the boundary zone was of a low temperature (below T_{MI}), the resistance and specific heat in the zone would have been less than those in

the center part (see Fig. 1 in Ref. 22 and Fig. 3 in Ref. 24), and thus more current would have been redistributed to the boundary zone. As a result, the Joule heat and low specific heat increased the boundary zone temperature more rapidly so that the temperature difference was compensated. Therefore, the second explanation alone does not satisfactorily explain the nonuniformity of the heating/conductance. Based on this consideration, we believe that the phase separation is responsible for the inhomogeneous heating/conductance. When approaching T_{MI} , the continuous ferromagnetic metal phase is separated from the paramagnetic insulating matrix. The current was distributed mainly in the continuous metallic ferromagnetic phases. As a result, only the conducting paths (around the ferromagnetic metallic phases) are expected to contribute to the measured conductance and are heated effectively. In our previous investigations, the same sample was found to be homogeneously ferromagnetic below T_C (205 K) based on magnetization, transport, and electron-spin-resonance measurements. However, the homogeneity might be broken by applying a current even if the external temperature remains below T_C . This may be due to a few possibilities. (1) One phase separation happened while the sample (or a part of it) was heated up to T_C due to the applied current. (2) The current distribution was possibly inhomogeneous even when the effective temperature was below T_C . According to the double exchange framework, the metallic conductance and ferromagnetic ordering in perovskite manganites are due to the transferring of e_g electrons between Mn^{3+} and Mn^{4+} sites. Without the applied electrical field, e_g electron hopping occurs with an equal possibility in all directions and establishes a homogeneous ferromagnetic phase. However, under an applied electric field, e_g electrons hop preferentially along the direction of the applied electric field. The oriented e_g electron hopping might result in an oriented distribution of $\text{Mn}^{3+}/\text{Mn}^{4+}$ ions considering the unequal ratio of $\text{Mn}^{3+}/\text{Mn}^{4+}$ (7:3). In other words, a current/field-induced optimized conducting phase might form and collect most of the current flowing through the sample under an external electric field. Further theoretical studies are needed.

Based on the arguments above, we summarize the following. (1) Due to the phase separation or the possible current/field-induced inhomogeneity, the applied current mainly passed through a specific part of the sample (current paths) and heated effectively the current paths. (2) In the remaining part of the sample (with a high resistivity), a very small current flowed and its heating was ascribed to the heat conduction from the current paths. Thus, two different temperature zones exist within the sample and the temperature varied sharply from a higher value in the current paths to a lower one in the remaining insulating parts. (3) The measured resistance from the V - I curves actually came mainly from the contribution of the current paths where almost all the current passed through. (4) The increase of the temperature in the current paths due to Joule heating increased the resistivity correspondingly so that the current was redistributed. It is apparent that the current paths can change due to an increase in the applied current.

Consider the heat equilibrium equation,

$$\frac{\partial u(r,t)}{\partial t} = j^2(r,t)\rho(r,t) - \nabla \cdot J_u(r,t), \quad (1)$$

where $u(r,t)$, $j(r,t)$, $\rho(r,t)$, and $J_u(r,t)$ are the energy density, current density, resistivity, and energy current density at a spatial-time point (r,t) , respectively. This equation can be rewritten as

$$\rho_m C_p(T) \frac{\partial T(r,t)}{\partial t} = j^2(r,t)\rho(T) - \nabla \cdot D(T) \nabla T(r,t), \quad (2)$$

where ρ_m is the mass density, $C_p(T)$ is the temperature-dependent specific heat of unit mass sample, and $T(r,t)$ is the local temperature at point (r,t) . Both the resistivity ρ and the heat diffusion coefficient D are supposed to be only dependent on the local temperature $T(r,t)$. Combining the heat equilibrium equation, material properties [$\rho(T)$ and $D(T)$], and the usual electromagnetic equations, in principle, the local temperature $T(r,t)$ and current distribution $j(r,t)$ can be solved under specific boundary conditions (here the external environment temperature, the applied voltage, and the total current). However, in this paper, we employ some approximations to discuss the nonuniformity under different conditions, rather than solving these equations exactly.

Based on the summaries above, we describe the sample simply consisting of two sections, the current paths and the remaining insulating part. For simplification, within each part, the temperature, resistivity, and current density are assumed to be uniform, and the interface between the two parts is simplified as a geometric surface. This means that the continuously varying physical variables (temperature, resistivity, and current density) are described as two discrete values, specifically temperatures of T and T_0 , resistivities of ρ and ∞ , as well as current densities of j and 0 within the current paths and the remaining insulating part, respectively. These simplifications are expected to give some insights into the nonuniformity of sample while applying a large current. Based on this simple model, after integrating Eq. (2) in the whole current paths, we obtain a heating-cooling equilibrium equation,

$$m(T)C_p(T) \frac{dT}{dt} = I(t)V(t) - \gamma(T)S(T)(T - T_0), \quad (3)$$

where $m(T)$, $C_p(T)$, $\gamma(T)$, and $S(T)$ are the effective mass, specific heat, Newtonian cooling coefficient, and the effective surface area of current paths at temperature T , respectively. Here, the change of current paths with time, dm/dt , should also contribute to the equilibrium equation. However, the contribution can be rewritten by replacing the mass and surface areas of current paths by their effective values. Equation (3) can be obtained if both m and S are thought to be their corresponding effective values. The application of the effective m and S values actually means a slightly different division between current paths and the remaining part in our present simple model, and this still gives a description of the topological characteristics of the current paths. At the MI transition point (threshold current I_c), under the thermal equilibrium, we have $dT/dt=0$ and

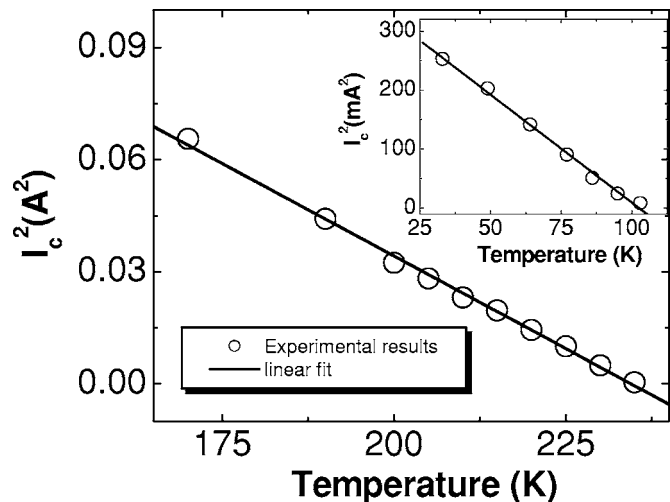


FIG. 2. The square of the threshold current (I_c^2) as a function of temperature, which is taken from the inset of Fig. 1(b) in Ref. 24. The inset shows a similar linear relationship between the square of the threshold current in the increasing current process and the external temperature in $(\text{La}_{0.3}\text{Pr}_{0.7})_{0.7}\text{Ca}_{0.3}\text{MnO}_3$ (data from the Fig. 3 of Ref. 18).

$$I_c^2 = a(T_{\text{MI}} - T_0). \quad (4)$$

This is simply the experimentally observed linear relationship between the square of the threshold current and the external temperature (see Fig. 2, which is taken from the inset of Fig. 1(b) in Ref. 24) with a coefficient of $a = \gamma(T_{\text{MI}}) \times [S(T_{\text{MI}})/R(T_{\text{MI}})]$. It indicates strongly that the heat accumulation is small at least while the current approaches I_c . From the fitted coefficient a , we obtained the cooling coefficient $b = \gamma S = 0.0008 \text{ J/K}$ at T_{MI} by using $R(T_{\text{MI}}) = 0.9 \Omega$ (see Fig. 1). It should be noted that in the phase-separated $(\text{La}_{0.3}\text{Pr}_{0.7})_{0.7}\text{Ca}_{0.3}\text{MnO}_3$,¹⁸ a similar linear relationship between the square of I_c and T_0 was also found, as shown in the inset of Fig. 2. This similar linear relation described in Ref. 18 can also be well explained by the similar model. Therefore, this implies that the present heat equilibrium model might describe some universal features of phase-separated systems under a large applied current.

In the resistance measurements performed on the same sample by applying a small current ($1 \mu\text{A}$),^{22,23} the real temperature T of current paths is the same as T_0 as is expected by the negligible Joule heating. In the present large current case, T is not equal to T_0 due to a large Joule heating contribution. However, if the effective temperature T is used, the resistivity-temperature relation $\rho(T)$ is approximately the same as that in the small current cases. We have calculated the effective temperature T of current paths from the $R(T)$ curve measured in a small current limit,

$$T = R^{-1}(V/I), \quad (5)$$

where $R^{-1}(V/I)$ is the reverse function of the $R(T)$ curve measured in the small current regime [Fig. 1 in Ref. 22 and Fig. 1(a) in Ref. 23], and V and I are the voltage and the applied current in the large current measurements, respectively. In addition, in our measurements, since the time dependence of the applied current $I(t)$ was linear, the calculated effective temperature $T(I)$ at each current I can be rewritten

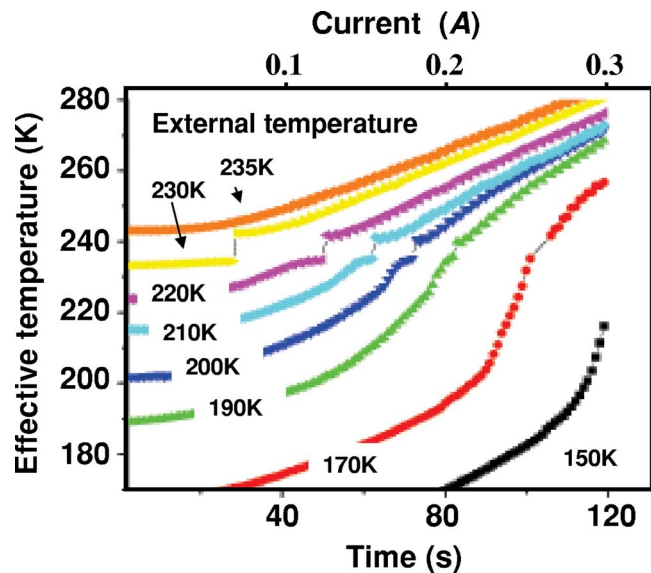


FIG. 3. (Color online) Effective temperature T of the current paths vs the applied current (I)/time (t).

as $T(t)$. The calculated results from Eq. (5) by using the measured I - V data at eight different external temperatures are shown in Fig. 3. All $T(t)$ or $T(I)$ curves are found to break at T_{MI} , and almost all dT/dt approach to zero at this point, which is in agreement with Eq. (4). Considering that the effective mass and surface area of the current paths are dependent on the effective temperature T , we can fit the parameters $C(T) = m(T)C_p(T)$ and $b(T) = \gamma(T)S(T)$ in Eq. (3) at any T by using the $T(t)$ curves. In the fitting procedure, for each selected T_0 value, we used appropriate $I(t)$, $V(t)$, $T(t)$, and dT/dt values obtained from the $T(t)$ curve. In order to minimize the fitting error, we used a few data points in a small temperature region ($T - \Delta/2$, $T + \Delta/2$) for each T_0 to get the average value of the parameters $C(T)$ and $b(T)$ at the small region around T , where Δ was chosen to be very small so that the parameters only varied slightly. In Fig. 4, we show the obtained $b(T)$, which is the product of the Newtonian cooling coefficient and the effective surface area of the current paths. We found that b increased by roughly one order of magnitude while increasing the temperature from 190 to 230 K. In the inset of Fig. 4, the effective mass of the current paths was also found to increase by about an order of magnitude, from 0.6 mg at 190 K to 6 mg at 233 K. However, the mass between the two electrodes for the voltage acquisition in V - I measurements was estimated to be ~ 37 mg. These results are clearly consistent with the partly heating/conducting description proposed above.

Additionally, oscillatory behavior of differential resistance (dV/dI) was observed and is shown in Figs. 5(a) and 5(b). At 240 and 245 K, i.e., slightly above the T_{MI} for zero magnetic field, oscillations in the differential resistance appeared at the current was higher than ~ 0.1 A. The oscillation period decreased with increasing temperature. At temperatures above 250 K, no clear oscillation was observed [see Fig. 5(c)]. The oscillation was closely dependent on the magnetic field (not shown here). Notably, it was also at 240 and 245 K where unusually large low-field magnetoresis-

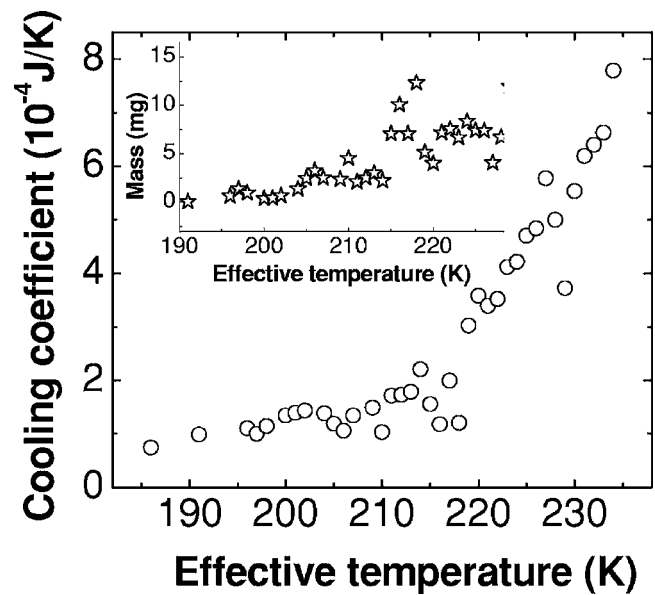


FIG. 4. The obtained cooling coefficient $b(T)$ as a function of the effective temperature of the current paths. The inset shows the mass of the current paths as a function of the effective temperature. Here, $m(T)$ is calculated from the fitted $C(T)$ and our measured specific heat $C_p(T)$ data (Ref. 24).

tance effects appeared (Ref. 22), which has been attributed to spin-dependent tunneling between isolated ferromagnetic clusters embedded in the insulating paramagnetic matrix. Therefore, it is reasonable to attribute the aforementioned oscillatory behaviors to electron tunneling.

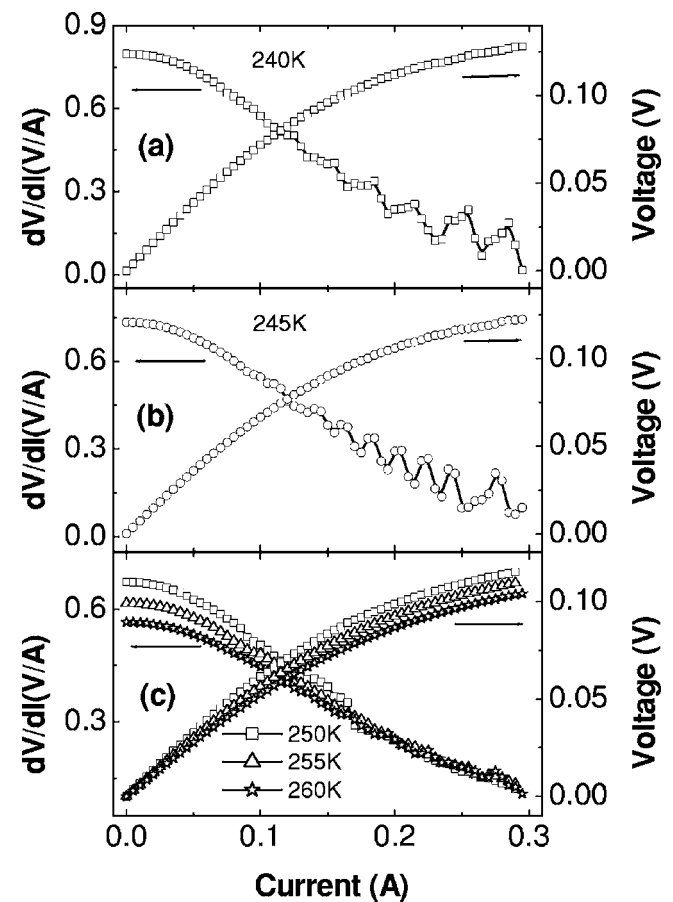


FIG. 5. Current dependence of the differential resistance (dV/dI) and voltage at 240 K (a), 245 K (b), and 250–260 K (c), respectively.

IV. SUMMARY

In summary, in electronically phase-separated $\text{Pr}_{0.7}\text{Pb}_{0.3}\text{MnO}_3$ single crystals, nonlinear current effects were found above a threshold current. The square of the threshold current decreased linearly with the external temperature. Using heat equilibrium theory, we have proposed a simple model to explain the experimental results and subsequently obtained insights into the topological characteristics of the current paths and their dependence on the applied current. More detailed studies based on the model are expected to give further insights into the phase-separated systems while applying an electrical current/field.

ACKNOWLEDGMENTS

One of authors (X.Z.) thanks the financial support of Alexander von Humboldt Foundation and also thanks Tokunaga for supplying their experimental data. The authors acknowledge the financial support from MEXT, Japan.

¹R. von Helmolt, J. Wecker, B. Holzapfel, L. Schultz, and K. Samwer, *Phys. Rev. Lett.* **71**, 2331 (1993).

²S. Jin, T. H. Tiefel, M. McCormack, R. A. Fastnacht, R. Ramesh, and L. H. Chen, *Science* **264**, 413 (1994).

³C. Zener, *Phys. Rev.* **82**, 403 (1951).

⁴E. Dagotto, T. Hotta, and A. Moreo, *Phys. Rep.* **344**, 1 (2001).

⁵A. Asamitsu, Y. Tomioka, H. Kuwahara, and Y. Tokura, *Nature (London)* **388**, 50 (1997).

⁶M. Fiebig, K. Miyano, Y. Tomioka, and Y. Tokura, *Science* **280**, 1925

(1998).

⁷J. Stankiewicz, J. Sese, J. Garcia, J. Blasco, and C. Rillo, *Phys. Rev. B* **61**, 11236 (2000).

⁸S. Srivastava, N. K. Pandey, P. Padhan, and R. C. Budhani, *Phys. Rev. B* **62**, 13868 (2000).

⁹Y. Yuzhelevski, V. Markovich, V. Dikovski, E. Rozenberg, G. Gorodetsky, G. Jung, D. A. Shulyatev, and Ya. M. Mukovskii, *Phys. Rev. B* **64**, 224428 (2001).

¹⁰J. Philip and T. R. N. Kutty, *Appl. Phys. Lett.* **79**, 209 (2001).

¹¹Y. Dikovski, Y. Yuzhelevski, V. Markovich, G. Gorodetsky, G. Jung, D. A. Shulyatev, and Ya. M. Mukovskii, *Phys. Rev. B* **65**, 144439 (2002).

¹²S. Merone, A. Wahl, C. Simon, and C. Martin, *Phys. Rev. B* **65**, 214428 (2002).

¹³P. Padhan, W. Prellier, C. Simon, and R. C. Budhani, *Phys. Rev. B* **70**, 134403 (2004).

¹⁴A. Odagawa, H. Sato, I. H. Inoue, H. Akoh, M. Kawasaki, Y. Tokura, T. Kanno, and H. Adachi, *Phys. Rev. B* **70**, 224403 (2004).

¹⁵A. Masuno, T. Terashima, Y. Shimakawa, and M. Takano, *Appl. Phys. Lett.* **85**, 6194 (2004).

¹⁶F. X. Hu and J. Gao, *Phys. Rev. B* **69**, 212413 (2004); *Appl. Phys. Lett.* **86**, 092504 (2005).

¹⁷Y. G. Zhao *et al.*, *Appl. Phys. Lett.* **86**, 122502 (2005).

¹⁸M. Tokunaga, Y. Tokunaga, and T. Tamegai, *Phys. Rev. Lett.* **93**, 037203 (2004).

¹⁹M. Tokunaga, H. Song, Y. Tokunaga, and T. Tamegai, *Phys. Rev. Lett.* **94**, 157203 (2005).

²⁰A. Palanisami, M. B. Weissman, and N. D. Mathur, *Phys. Rev. B* **71**, 094419 (2005).

²¹T. Wu and J. F. Mitchell, *Appl. Phys. Lett.* **86**, 252505 (2005).

²²R.-W. Li *et al.*, *Appl. Phys. Lett.* **80**, 3367 (2002).

²³R.-W. Li, X. Zhou, B.-G. Shen, and B. Hillebrands, *Phys. Rev. B* **71**, 092407 (2005).

²⁴R.-W. Li, X. Zhou, A. Belik, K. Miki, and B. G. Shen, *J. Appl. Phys.* **99**, 08Q301 (2006).